

Article

Numerical Investigation of Flow and Structural Characteristics of a Large High-Head Prototype Pump–Turbine during Turbine Start-Up

Xilong Yin ¹, Xingxing Huang ², Shaozheng Zhang ¹, Huili Bi ¹ and Zhengwei Wang ^{1,*}

¹ Department of Energy and Power Engineering, Tsinghua University, Beijing 100084, China; yinxl21@mails.tsinghua.edu.cn (X.Y.)

² S.C.I. Energy, Future Energy Research Institute, Seidengasse 17, 8706 Zurich, Switzerland

* Correspondence: wzw@mail.tsinghua.edu.cn

Abstract: Transient processes that occur in pumped storage power plants can cause high-pressure conditions, which in turn can result in vibrations in the pump–turbine structure and even damage to structural components. It is therefore crucial to research the transient process of the large pump–turbine units and the flow-induced vibrations of the structural components. The three-dimensional flow field and structural field models of a high-head prototype pump–turbine were constructed to study its flow characteristics and structural characteristics under the turbine start-up. Calculations and analyses were performed on the pressure variation and the flow-induced stress concentrations of the pump–turbine during start-up in turbine mode. The simulated pressure distributions during the turbine start-up were mapped onto the finite element calculation model of the structures of the pump–turbine to calculate the flow-induced stress concentrations. This study provides a reference to improve the design and operation of high-head prototype pump–turbines based on the findings of the flow and structural characteristics.

Keywords: pump–turbine; flow and structural characteristics; fluid–structure coupling; turbine start-up; stress concentration



Citation: Yin, X.; Huang, X.; Zhang, S.; Bi, H.; Wang, Z. Numerical Investigation of Flow and Structural Characteristics of a Large High-Head Prototype Pump–Turbine during Turbine Start-Up. *Energies* **2023**, *16*, 3743. <https://doi.org/10.3390/en16093743>

Academic Editor: Helena M. Ramos

Received: 19 March 2023

Revised: 25 April 2023

Accepted: 26 April 2023

Published: 27 April 2023



Copyright: © 2023 by the authors. Licensee MDPI, Basel, Switzerland. This article is an open access article distributed under the terms and conditions of the Creative Commons Attribution (CC BY) license (<https://creativecommons.org/licenses/by/4.0/>).

1. Introduction

With the increasing demand for power and the pressure of environmental protection in recent years, solar and wind energy have become crucial renewable energy sources in many countries. As clean energy has become more accessible to the grid, demand for grid peak and frequency regulation has increased. Pumped storage hydropower has become increasingly popular around the world due to its flexible features.

An upper reservoir, diversion tunnels, a pump–turbine, tailwater tunnels, and a lower reservoir comprise a hydraulic pumped storage power plant, and the pump–turbine is the heart of the entire pumped storage power plant. The water in the upper reservoir flows down and drives the runner to generate power when the pump–turbine units operate in turbine mode. In pump mode, the pump–turbine units pump water from the lower reservoir to the upper reservoir to store the power.

The pumped storage power plant generally has a high water head, long diversion tunnels, and a narrow vaneless space. During the transient process, there are huge fluctuations of pressure in the narrow vaneless space that induce large deformation and stress on the structural parts. The start-up process produces larger static stress and dynamic stress than normal operating conditions [1–3]. As a result of the high-level pressure fluctuation, the pump–turbine may be stressed and deformed, causing it to fail or become damaged. The research shows that the stress fluctuation during the start-up and shutdown of the pump–turbine can be much larger than the rated operating conditions and cause damage to the runner of the pump–turbine [4–6]. In addition to the fatigue damage of

rotating parts such as runners, the static structure of pumped storage units also suffer from stress concentration and excessive deformation [7–9]. Researchers summarized the phenomenon of vibration in the water guide mechanism of pumped storage power plants and analyzed the causes of fracture of the head cover connecting bolts in the fixed components [10–15]. Therefore, it is of vital importance to investigate the turbine start-up of the pump–turbine, and the flow and the structural characteristics of the pump–turbine unit during the turbine start-up.

Since unit model tests and prototype tests are usually costly and inconvenient, numerical simulations have become an effective method for the investigation of flow characteristics and structural characteristics of pump–turbines. With numerical simulations, the most important thing to consider is the accuracy compared to prototypes and model tests. Numerical simulations of pump–turbine sets have been the subject of many studies to verify their reliability by comparing calculations with field measurements. At present, scholars have published much research work on pump–turbine flow, and a certain scale has been formed in the direction of numerical simulation and calculation. The law of the pump–turbine dynamic and static interference phenomenon has been summarized [16,17]. The researchers summarized the dynamic and static interference model according to numerical simulation and experimental results, and summarized the main frequency and variation law of pressure pulsation in the vaneless area [18–20]. The study of flow characteristics under steady-state conditions is mostly focused on the unit itself, while the study of flow characteristics of transient processes such as start-up and shutdown involves the power station piping line system. When the unit undergoes a transient process, the changes of pressure wave and flow rate in the power station pipeline will also have an impact on the flow characteristics of the unit. Therefore, some scholars adopt the research method of combining the one-dimensional characteristic line method with the three-dimensional flow calculation, and use the inlet and outlet hydraulic characteristics such as pressure and flow rate obtained from the one-dimensional calculation of the pipeline as the boundary conditions of the three-dimensional flow calculation of the unit, so as to realize the solution of the structural response of the unit. [21,22]. Researchers have further confirmed the reliability of the numerical investigation according to the field measurement data for the turbine start-up of the pump–turbine units [23,24]. The results show that under the condition of limited computational resources, selecting key time points for static calculations is an efficient means to analyze the flow characteristics of the unit during the transient process. The results show that errors are within project-acceptable ranges.

In this paper, firstly we constructed a complete fluid domain model and a structural domain model of a large high-head prototype pump–turbine. The fluid domain model includes the main parts such as spiral case, stay vane, guide vane, balance pipes, runner and draft tube, as well as the flow gap model between the runner and head cover, and the runner and bottom ring. The structural field model includes the structural model of the runner and the structural model of fixed components such as the head cover, stay ring, and bottom ring. One-dimensional pipeline calculation was performed for fluid calculations during turbine start-up. In the following step, the flow characteristics during turbine start-up were analyzed by coupling flow domain calculations. We used the one-way fluid–structure coupling method to map the obtained pressure files to structural components. Finally, the structural characteristics were analyzed. The structural safety is evaluated and the stress concentration and deformation distribution of runners and fixed components affected by hydraulic excitation are summarized. The change pattern of structural field dynamic characteristics in the transient process of turbine start-up is investigated, and improvement solutions are proposed for structural hazard situations such as stress concentration and excessive deformation. The results of this research can provide valuable references for optimizing hydraulic turbine designs.

2. Numerical Calculation Method

In this research, numerical calculation methods include the three-dimensional (3D) fluid dynamics method, 1D pipeline calculation method, and the fluid–structure coupling method.

2.1. The 3D Flow Simulation Governing Equations and the Turbulence Model

When simulating the internal flow field of hydraulic machinery such as a pump–turbine, the change in density of the flow medium can be ignored and the flow of a low-speed fluid can be approximated as the turbulent flow of a three-dimensional incompressible fluid. The conserved differential form of the Navier–Stokes (N-S) equations is described as follows:

$$\frac{\partial \rho}{\partial t} + \frac{\partial}{\partial x_i} (\rho u_i) = 0 \quad (1)$$

$$\frac{\partial}{\partial x_j} (\rho u_i u_j) + \frac{\partial}{\partial t} \rho u_i = \frac{\partial \tau_{ij}}{\partial x_j} - \frac{\partial p}{\partial x_i} + \rho f_i \quad (2)$$

$$\tau_{ij} = - \left(\frac{2}{3} \mu \frac{\partial u_j}{\partial x_j} + p \right) \delta_{ij} + \mu \left(\frac{\partial u_i}{\partial x_j} + \frac{\partial u_j}{\partial x_i} \right), \quad \delta_{ij} = \begin{cases} 1, & i = j \\ 0, & i \neq j \end{cases} \quad (3)$$

where ρ , u , and p are the density, velocity, and pressure of fluid, τ is the surface force tensor, and i and j represent directions. The Reynolds Averaged N-S equations are the appropriate approximation and simplification of turbulent flows:

$$\frac{\partial}{\partial x_i} (\bar{u}_i) = 0 \quad (4)$$

$$\frac{\partial}{\partial t} (\bar{u}_i) + \frac{\partial}{\partial x_j} (\bar{u}_i \bar{u}_j) = \frac{\partial}{\partial x_j} \left[\nu \left(\frac{\partial \bar{u}_i}{\partial x_j} + \frac{\partial \bar{u}_j}{\partial x_i} \right) \right] - \frac{1}{\rho} \frac{\partial \bar{p}}{\partial x_i} - \frac{\partial \overline{u'_i u'_j}}{\partial x_i} + f_i \quad (5)$$

By subtracting the RANS equations from the N-S equations, the equations of motion for turbulent pulsations are

$$\frac{\partial}{\partial x_i} (u'_i) = 0 \quad (6)$$

$$\frac{\partial u'_i}{\partial t} + \bar{u}_j \frac{\partial u'_i}{\partial x_j} + u'_j \frac{\partial \bar{u}_i}{\partial x_j} = \frac{\partial}{\partial x_j} \left[\nu \left(\frac{\partial u'_i}{\partial x_j} + \frac{\partial u'_j}{\partial x_i} \right) \right] - \frac{1}{\rho} \frac{\partial p'}{\partial x_i} - \frac{\partial}{\partial x_j} (u'_i u'_j - \overline{u'_i u'_j}) \quad (7)$$

In order to close the RANS equations, the SST k - ω turbulence model is used. Considering the turbulent energy k and the turbulent frequency ω , the transport equations are given below:

$$\frac{\partial k}{\partial t} + \frac{\partial}{\partial x_j} (\bar{u}_j k) = \frac{\partial}{\partial x_j} \left[\left(\nu + \frac{\nu_t}{\sigma_{k1}} \right) \frac{\partial k}{\partial x_j} \right] + P_k - \beta' k \omega \quad (8)$$

$$\frac{\partial \omega}{\partial t} + \frac{\partial}{\partial x_j} (\bar{u}_j \omega) = \frac{\partial}{\partial x_j} \left[\left(\nu + \frac{\nu_t}{\sigma_{\omega 1}} \right) \frac{\partial \omega}{\partial x_j} \right] + \alpha_1 \frac{\omega}{k} P_k - \beta_1 \omega^2 \quad (9)$$

The SST k - ω turbulence model is widely used as it can better predict flow separation in the region of the inverse pressure gradient.

$$\frac{\partial k}{\partial t} + \frac{\partial}{\partial x_j} (\bar{u}_j k) = \frac{\partial}{\partial x_j} \left[\left(\nu + \frac{\nu_t}{\sigma_{k2}} \right) \frac{\partial k}{\partial x_j} \right] + P_k - \beta' k \omega \quad (10)$$

$$\frac{\partial \omega}{\partial t} + \frac{\partial}{\partial x_j} (\bar{u}_j \omega) = \frac{\partial}{\partial x_j} \left[\left(\nu + \frac{\nu_t}{\sigma_{\omega 2}} \right) \frac{\partial \omega}{\partial x_j} \right] + (2 - 2F_1) \frac{1}{\sigma_{\omega \omega}} \frac{\partial \omega}{\partial x_j} \frac{\partial k}{\partial x_j} + \alpha_2 \frac{\omega}{k} P_k - \beta_2 \omega^2 \quad (11)$$

where $\nu = k/\omega$, $\alpha_1 = 0.56$, $\alpha_2 = 0.44$, $\beta_1 = 0.075$, $\beta_2 = 0.0828$, $\beta' = 0.09$, $\sigma_{k1} = 2$, $\sigma_{k2} = 1$, $\sigma_{\omega 1} = 2$, $\sigma_{\omega 2} = 1.168$.

2.2. The 1D Pipeline Calculation Method

In this paper, the 1D characteristic line method was used to simulate the pressure wave transfer within a pipeline system of a pump–turbine power station during its transient processes. The transient calculation of pipelines is described in detail below.

We can assume that the pipeline has an unsteady flow in 1D during its transient period. The control equation is

$$\frac{1}{\rho} \frac{\partial p}{\partial x} + \frac{\partial u}{\partial t} + u \frac{\partial u}{\partial x} + g \sin \alpha + \frac{\lambda u |u|}{2D} = 0 \quad (12)$$

$$\rho a^2 \frac{\partial u}{\partial x} + \frac{\partial p}{\partial t} + u \frac{\partial p}{\partial x} = 0 \quad (13)$$

where λ is the coefficient of friction of the pipe, α is the slope of the pipe, D is the internal diameter of pipes, and a is the wave velocity.

The solution can be transformed into discrete differential equations on characteristic lines, and the two sets of characteristic lines and their compatibility equations are as follows:

$$C^+ : \begin{cases} \frac{1}{a} \frac{dH}{dt} + \frac{1}{gA} \frac{dQ}{dt} + \frac{\lambda Q |Q|}{2gDA^2} = 0 \\ \frac{dx}{dt} = +a \end{cases} \quad (14)$$

$$C^- : \begin{cases} -\frac{1}{a} \frac{dH}{dt} + \frac{1}{gA} \frac{dQ}{dt} + \frac{\lambda Q |Q|}{2gDA^2} = 0 \\ \frac{dx}{dt} = -a \end{cases} \quad (15)$$

Iterations can be completed by integrating the equations into differential form by modifying the flow velocity and head between two points.

2.3. Structural Governing Equations

In order to establish the finite element control equations for the structural dynamics, the following equation is obtained using D'Alembert's principle:

$$\int \delta \varepsilon^T \sigma_s dV = \int_V \delta x^T (f_s - \rho_s \ddot{x} - \mu_s \dot{x}) dV \quad (16)$$

where ρ_s is structure density, x is structural displacement, \dot{x} is velocity, \ddot{x} is accelerated speed, σ_s is Cauchy stress tensor, and f_s is structural volume force.

After discretization of the above equations using finite elements, the discrete structural dynamics equation can be expressed as follows:

$$M_s \ddot{x} + N_s \dot{x} + K_s x = F_s \quad (17)$$

where M_s is mass matrix, N_s is damping matrix, K_s is stiffness matrix, and F_s is the load vector.

Taking the pressure distributions of 3D flow calculations as the load input, a fluid-induced stress analysis of the water pump–turbine can be conducted. The structural stress is expressed as

$$\sigma = ESx \quad (18)$$

where E and S are the elasticity matrix and the strain–displacement matrix.

The evaluation of the pump–turbine structure's stress characteristics is based on von Mises stress.

$$\sigma_{vM} = \sqrt{\frac{(\sigma_1 - \sigma_2)^2 + (\sigma_2 - \sigma_3)^2 + (\sigma_3 - \sigma_1)^2}{2}} \quad (19)$$

where σ_1 , σ_2 , and σ_3 are the principal stresses.

3. Calculation Model of The Pump–Turbine

Figure 1 shows the sketch of the full system in this research. The whole system includes the upper reservoir, the lower reservoir, the diversion pipeline, the tailwater pipeline, and the main body of the flow calculation: the pump–turbine.

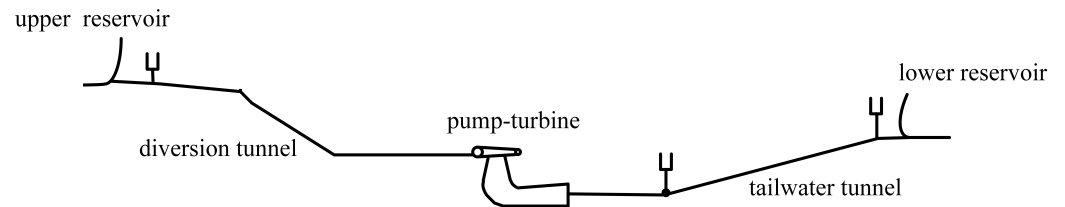


Figure 1. Sketch of the full system.

This study focuses on the flow field characteristics and structural characteristics of the turbine start-up process, and the calculations are based on a real power station, the sketch of the course line of the turbine start-up process is shown in Figure 2 below. The relevant parameters have been normalized due to the confidentiality needs of the power station. From this curve, the variation of the flow rate, guide vane opening, and other parameters of the turbine start-up process required for subsequent calculations can be obtained.

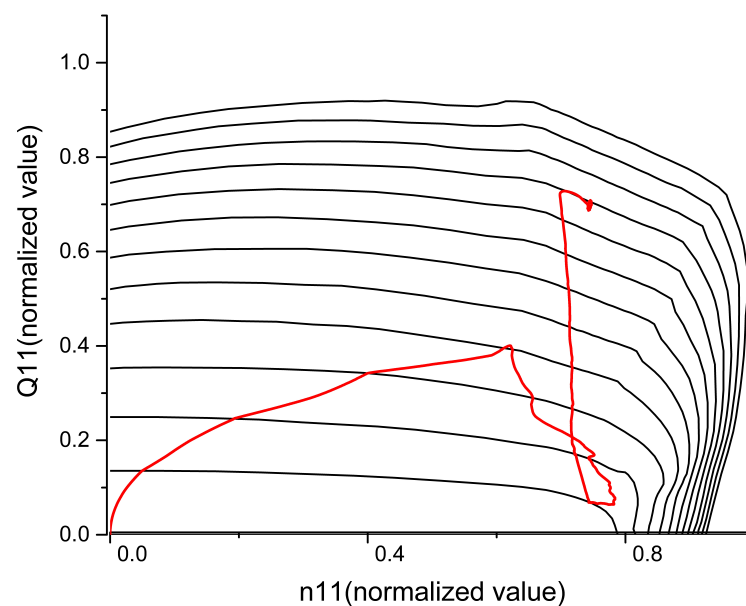


Figure 2. The start-up course line of the turbine.

3.1. Pump–Turbine Flow Model

In this study, a prototype pump–turbine unit with a high water head is studied. Figure 3 shows the full three-dimensional fluid domain calculation model, which includes stay vanes, runner, guide vanes, the spiral case, balance pipes, and the draft tube.

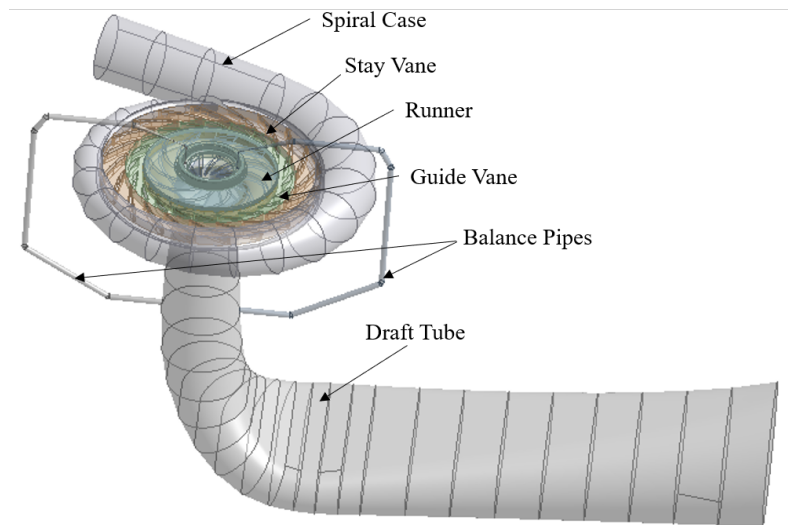


Figure 3. The full 3D flow computational domain.

The rated head of the PT unit is 545 m, the rated speed is 428.6 r/min, the rated output at the rated head is 357.1 MW. There are 11 blades in the runner, 20 stay vanes, and 20 guide vanes in the pump–turbine unit. Table 1 shows the main parameters of the unit during turbine mode operation.

Table 1. The main parameters of the pump–turbine unit.

Parameter	Unit	Value
Rated head Hr	m	545
Rated speed Nr	rpm	428.6
Unit capacity	MW	357.1
Runner blades	-	11
Stay vanes	-	20
Guide vanes	-	20

Based on the flow characteristics and geometry of each component, structured hexahedral mesh and unstructured tetrahedral mesh were chosen to delineate the fluid domain. The mesh quality was checked, and the meshes of each region met the calculation requirements. The meshes of each part of the fluid domain are shown in Table 2.

Table 2. Elements numbers of the 3D flow domains.

Flow Domain	Elements Number ($\times 10^6$)
Spiral case	1.80
Runner	1.34
Stay vane	1.37
Guide vane	0.25
Draft tube	0.14
Pressure-balanced pipes	0.25
Total	5.15

The fluid dynamics calculations were performed on ANSYS CFX, with a total analysis time of 1.4 s, including 10 rotations of the runner. Rotation was set at 428.6 rpm for the runner region, while stationary settings were set for the other fluid regions. The inlet boundary condition is set to the total pressure of the spiral case and the outlet boundary condition is set to the static pressure of the draft tube. The no-slip boundary condition is set as the wall boundary condition. There are transient rotor–stator interfaces between the

guide vane region and runner region, and between the runner region and tailpipe region. The residuals were set to 10^{-4} . For the purpose of verifying mesh independence, three sets of meshes were constructed. The mesh of the draft tube, guide vane, and runner can all be adjusted independently. During turbine start-up, the relative torque is selected in order to check the mesh's independence. Based on the findings displayed in Figure 4, the mesh with 5,159,129 elements was used for the following study.

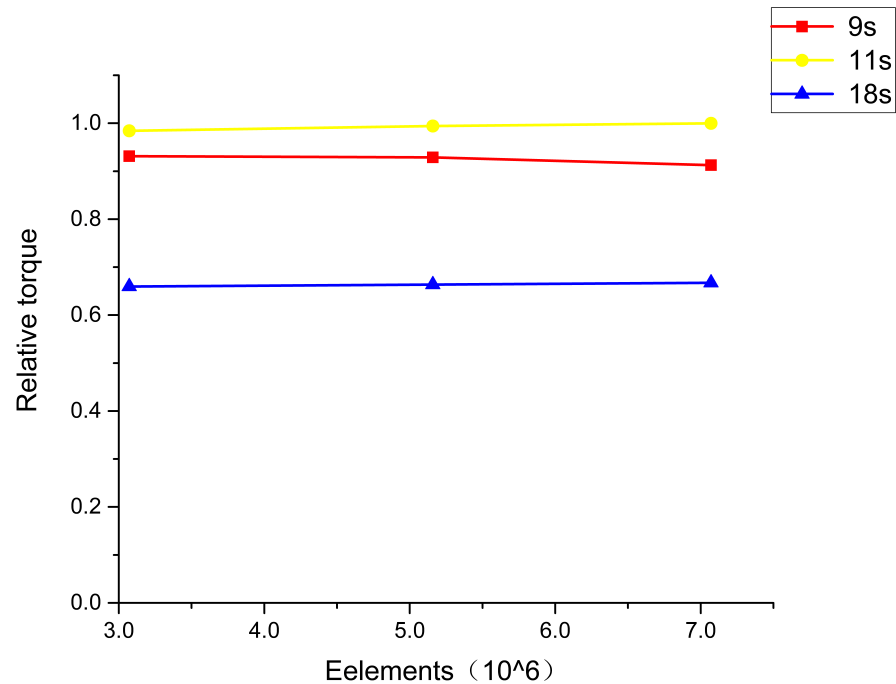


Figure 4. Fluid mesh independence analysis.

3.2. Pump–Turbine Structural Model

The pump–turbine structural model includes a runner and fixed components such as the head cover. The mesh of the runner is shown in Figure 5 and the mesh of the structural model is shown in Figure 6. Considering the influence of external conditions on the runner, the rotation speed, gravity, and fixed constraints are applied to the runner model, and the material parameters of the runner are set with a yield strength of 250 MPa.

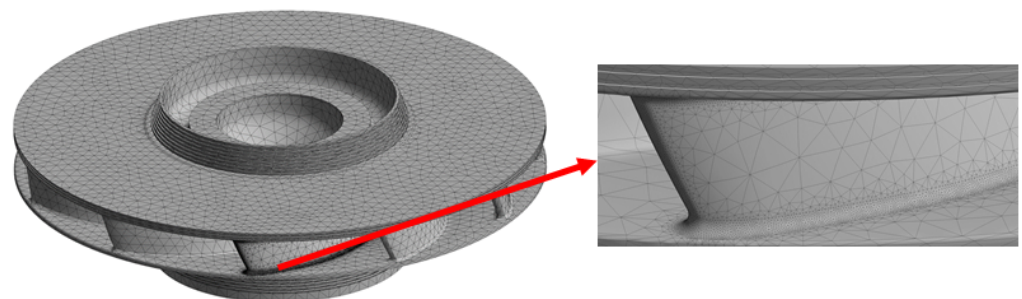


Figure 5. Mesh of the runner.

Considering the influence of external conditions on the fixed components, the bottom ring and the concrete connection part are all subjected to fixed constraints, and the yield strength is 335 MPa. The mesh of runner and stay vanes near the band and the crown are refined to increase the accuracy of the calculation results. The pressure loads calculated in

the flow field are mapped to this model to calculate the stresses and deformations in the runner and fixed components.

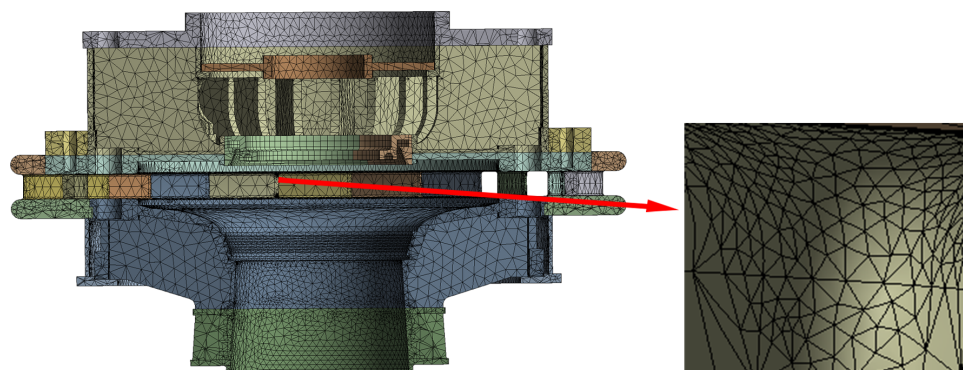


Figure 6. Structural mesh of the pump-turbine unit.

In order to observe the structural field response under turbine start-up process, three meshes with different numbers of nodes were divided for the structural field. Furthermore, a mesh sensitivity study was conducted under turbine start-up process, using equivalent stress as the comparison parameter (Figure 7). Based on the calculation results and the calculation time, the final mesh was determined.

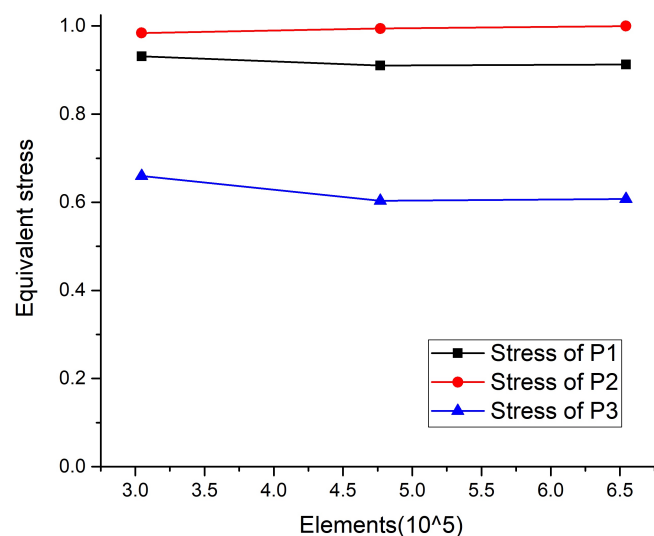


Figure 7. Mesh sensitivity study.

3.3. The 1D Pipeline Model

In the pipeline system, the 1D characteristic line method simulates the pressure wave transmission during turbine start-up. Flow rate, rotation speed, and opening of guide vanes are obtained by 1D calculation. The curves with time are shown in Figure 8. The parameters are normalized to the rated values of the turbine operating conditions. At 0–100 s is the unit start, and at 100 s the unit reaches no-load; at 100–200 s the process of increasing the load of the unit occurs, and the guide vane opens linearly. At the initial stage of the turbine start-up process, the guide vane opens, and the rotation speed and flow rate of the unit rise rapidly; then, in order to avoid the rotation speed exceeding the rated value of the turbine mode, the guide vane closes rapidly, so that the rotation speed is stabilized at the rated speed. When the unit completes grid connection, it starts to experience the process of increasing load, at which time the guide vane opens again and the flow rate also rises

gradually until it is stabilized. Then the start-up process ends, and the unit runs at the turbine's rated working condition.

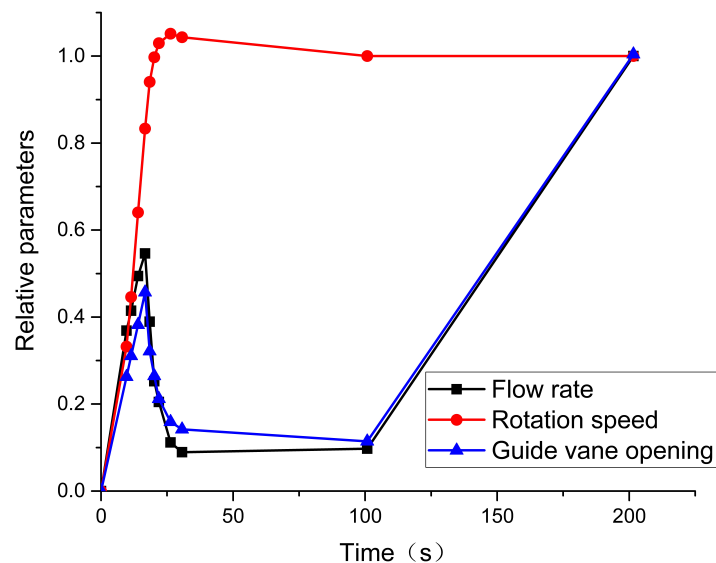


Figure 8. The flow rate, rotation speed, and guide vane opening during turbine start-up.

Figure 9 shows the relative pressures of the spiral case inlet and the draft tube outlet during turbine start-up. For the 3D fluid simulation, key time points are selected on the curves at extreme points. The researchers of [25–30] used a similar approach for fluid simulation. Pressures of the spiral case inlet and the draft tube outlet are used as boundary conditions for the 3D flow calculation.

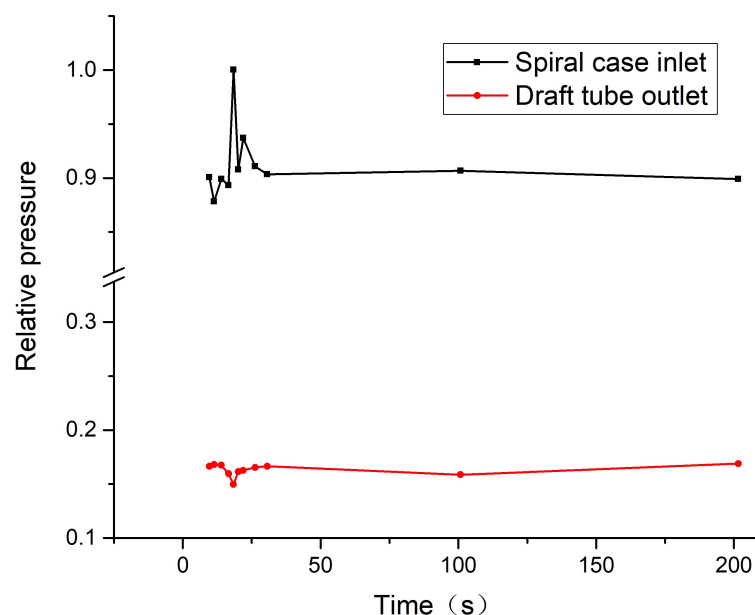


Figure 9. Relative pressure of inlet and outlet at the 11 key time points.

4. Results and Discussion

4.1. Flow Characteristics of the Pump–Turbine Unit

4.1.1. Pressure Change in the Runner Passages

As the turbine starts up, pressure changes in the runners are shown in Figure 10. The data were normalized to the maximum pressure value during turbine start-up to facilitate the study of pressure trends.

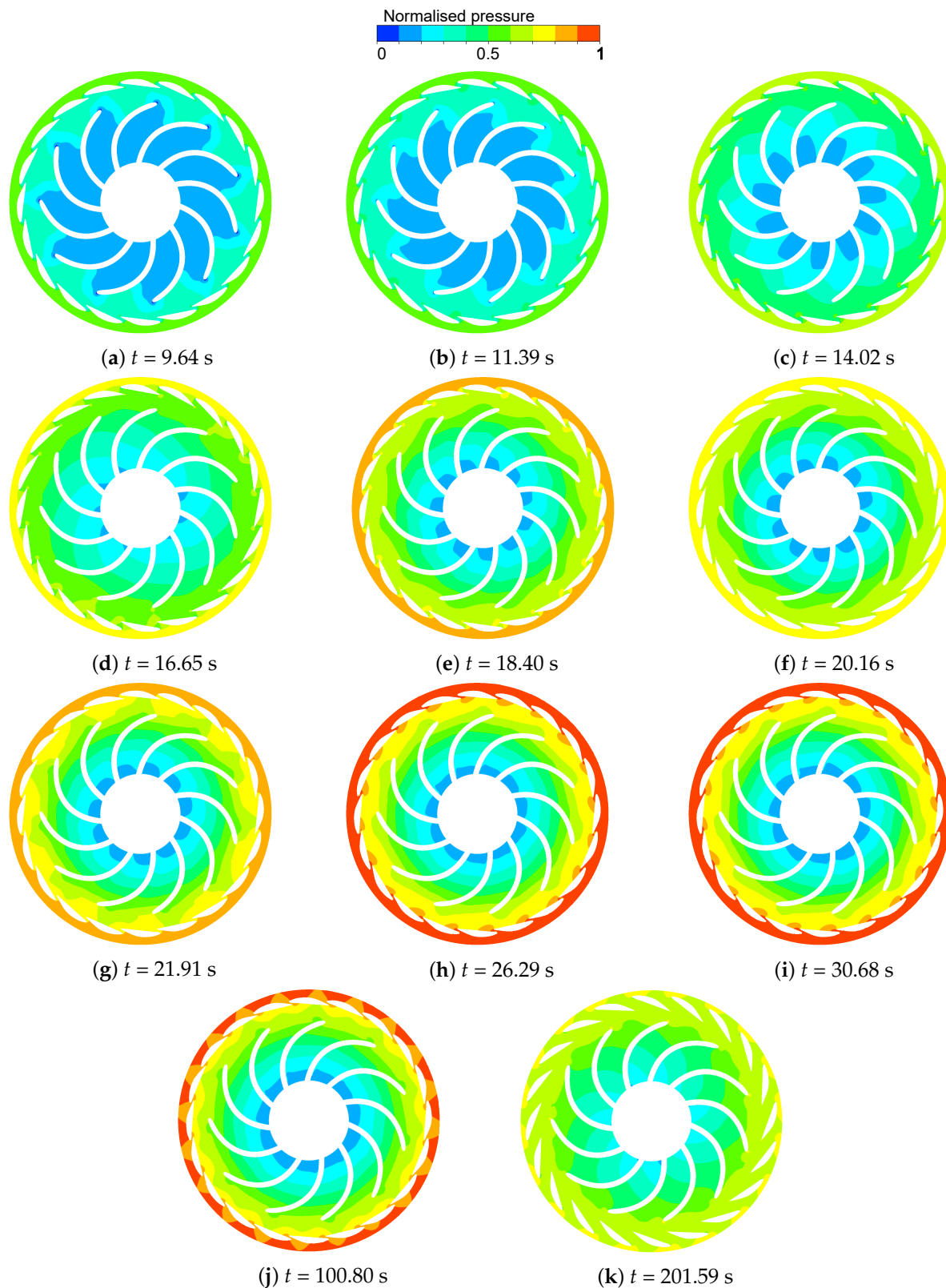


Figure 10. Pressure distribution at different time points.

In the first stage of the turbine start-up process, the guide vane opening increases, and the unit flow rate and speed gradually increases. The pressure of the runner and the guide vane also gradually increases, the fluid flow through the guide vane area after the pressure begins to drop significantly. In the second stage of the turbine start-up process,

the unit speed continues to rise. At this time, in order to avoid the speed exceeding the rated value of the turbine's working condition, the guide vane is quickly closed and the unit runs in the no-load operation area. In the second stage, the flow rate and torque of the turbine decrease due to the closing of the guide vane. In the third stage of the turbine start-up process, the unit is connected to the grid and starts to enter the process of increasing the load. The guide vane opens again until the opening of the guide vane is close to the rated working condition of the turbine, and the pressure between the guide vane and the runner flow field gradually decreases and stabilizes in this stage, and the unit finally enters the rated working condition for stable operation. When the water flows through the guide vanes, the pressure drops dramatically and a water ring forms between the runner and guide vanes. The complex vortex structure is in the runner passages because of flow separation and backflow, as shown in Figure 11. The pressure data were normalized to the maximum pressure value during turbine start-up.

By closing the guide vane slightly as the speed approaches the rated speed, this pump-turbine operates in the no-load operating zone and the runner begins to stabilize around the rated speed. During this process, the guide vane opening decreases and the energy of the water ring becomes strong and surrounds the entire vaneless space, forming a ring of water resistance in the circumferential direction. The large vortex inside the runner gradually stretches along the flow direction and breaks down into two vortices in the flow direction. The outer circumference of the runner is wrapped in a high-speed ring, blocking the upstream flow, and the flow inside the runner is very turbulent. In the water ring with the water-blocking effect and the runner vortex with the blocking effect, there is a combined effect, so the flow and torque drop.

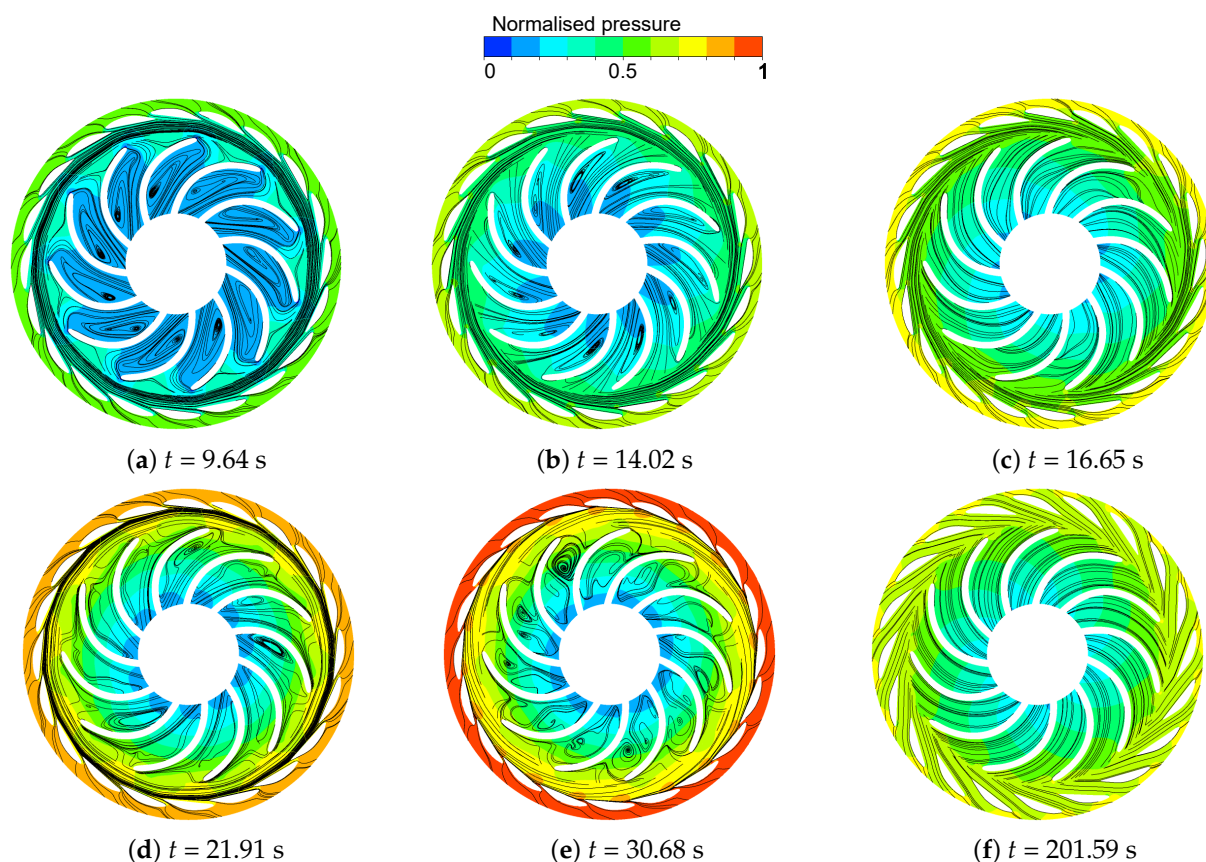


Figure 11. Streamlines in the guide vanes and runner passage at six key time points.

Following that, the guide vane is reopened and gradually increased in opening degree to reach the rated working condition, and the pressure in the runner and guide vane is gradually stabilized.

4.1.2. Axial Thrust of Runner

As shown in Figure 12, when starting up a turbine, the runner's relative axial thrust increases dramatically as the speed increases, reaching a maximum at 26 s and then gradually decreasing and stabilizing. The data were normalized according to the maximum axial thrust during turbine start-up.

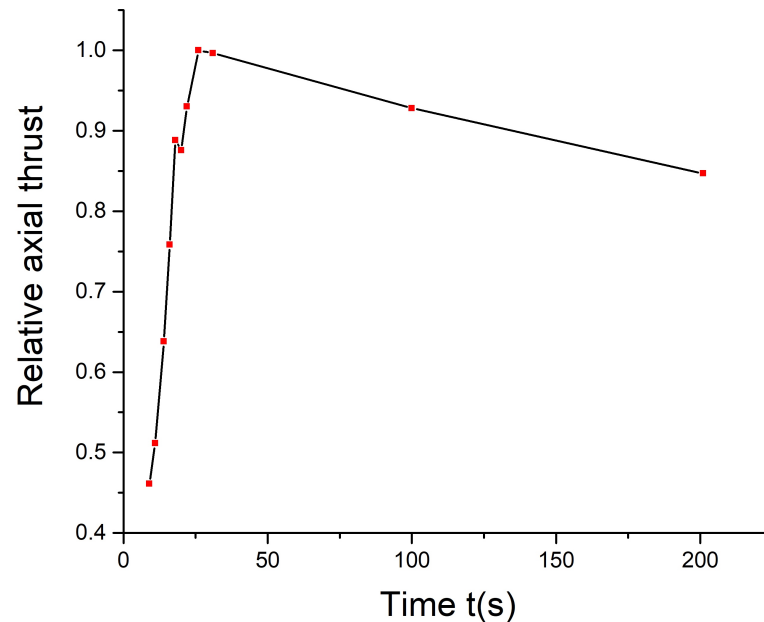


Figure 12. The runner's relative axial thrust during the turbine start-up process.

4.2. Structural Characteristics of the Pump–Turbine Unit

Through the above simulation, the pressure load is mapped onto the structural field. Gravity, rotation speed, and fixed constraints are applied to the surface of the structure, and stresses and deformations are calculated.

4.2.1. Stress and Deformation of the Runner

The guide vanes open gradually during the initial start-up stage. It can be seen in Figure 13 that the deformation is relatively evenly distributed, and the overall deformation is not significant. The data were normalized according to the maximum deformation of the runner during the turbine start-up process. Gradually increasing flow rates and speeds increase the deformation near the runner blades. A few seconds after the rotor speed stabilizes, the pressure gradually stabilizes. The turbine start-up ends, and the runner starts to deform less. Turbine blade deformation increases gradually as the turbine starts up, with inlet deformations significantly greater than outlet deformations.

The equivalent stress of the runner is shown in Figure 14, the inlet side and the outlet side is a more concentrated areas of stress. In a single runner blade, the maximum stress is usually found at the blade inlet side.

At each key time point, the runner's maximum equivalent stress is measured, as shown in Figure 15. The initial start-up causes the equivalent stress to increase and then decrease. When the guide vane's opening increases, the maximum equivalent stress reaches 123.5 MPa at 100 s. This value is less than the runner material yield strength of 250 MPa, so the runner components are considered safe during the turbine start-up process.

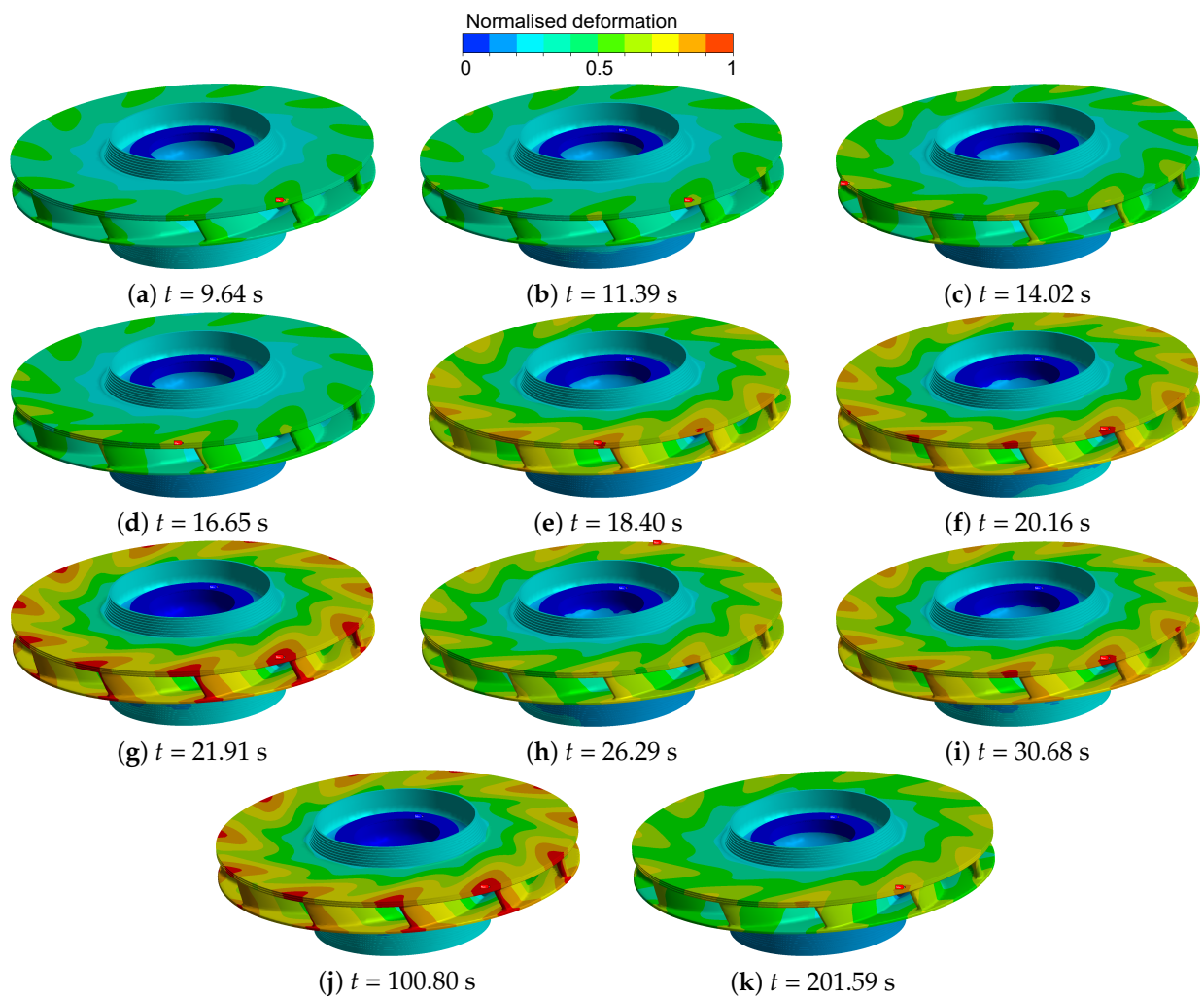


Figure 13. Total deformation distribution of the runner.

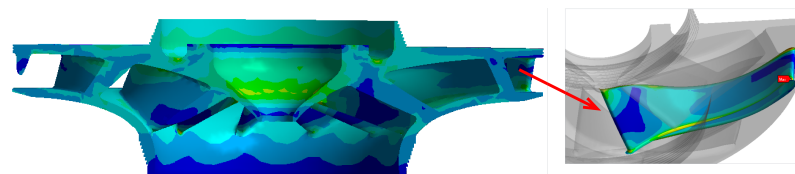


Figure 14. Equivalent stress of runner during turbine start-up.

4.2.2. Stress and Deformation of Stationary Structures

During turbine start-up, the deformation distribution is shown in Figure 16. The data were normalized according to the maximum deformation of stationary structures during turbine start-up. Pump-turbine units suffer from maximum deformation at the inner head cover, which also causes vibration and noise. A large axial thrust is generated by the hydraulic pressure acting on the head cover's inside surface. This results in a large deformation of the head cover.

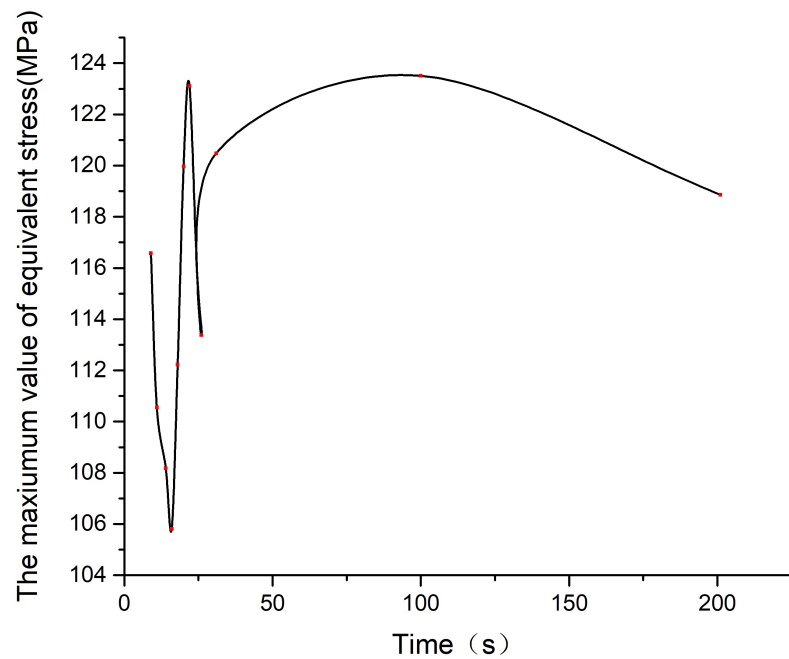


Figure 15. The maximum equivalent stress of the runner during turbine start-up.

Normalised deformation

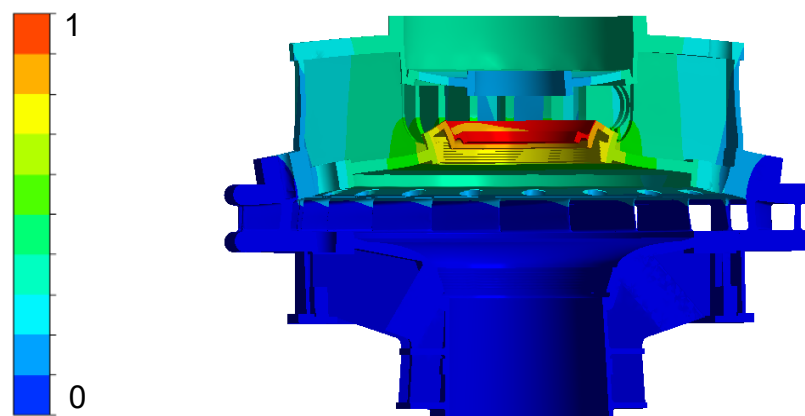


Figure 16. Deformation distribution of the stationary structure.

Axial support is provided by the stay ring, which is subject to high-pressure water flow. Figure 17 shows the normalized stress distribution of head cover. The data were normalized according to the maximum stress on the head cover during turbine start-up. There is the greatest amount of stress at the root of the ribbed plates. The maximum stress value of the head cover during the turbine start-up is 157.54 MPa, which is lower than the material yield limit of 335 MPa. The head cover is considered structurally safe.

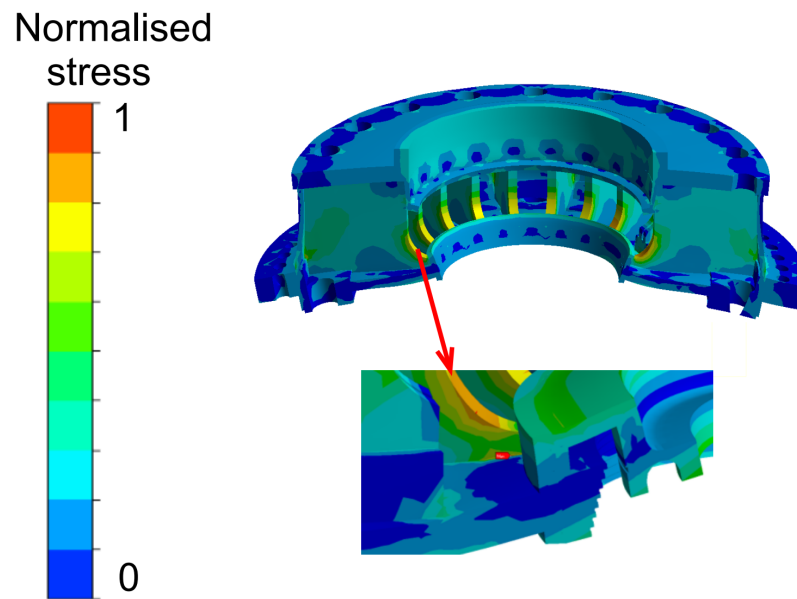


Figure 17. Stress distribution of head cover.

As a result of the pressure within the stationary structure, the head cover is pushed upwards, the bottom ring is pushed downwards, and the stay ring is stretched upward and downward. The stresses in the stay ring are mainly concentrated in the stay vane and the focus needs to be on improving the stress concentration in the stay vane. The maximum pressure occurs at the rounded corners on the outlet side of the stay vane of the stay ring, as shown in Figure 18. The data were normalized according to the maximum stress on the stay ring during turbine start-up. The maximum stress value of the stay ring during turbine startup is 514 MPa, and there is a risk of fatigue damage, which can be considered by increasing the radius of the inverted circle of the stay vane and the length or thickness of the stay vane.

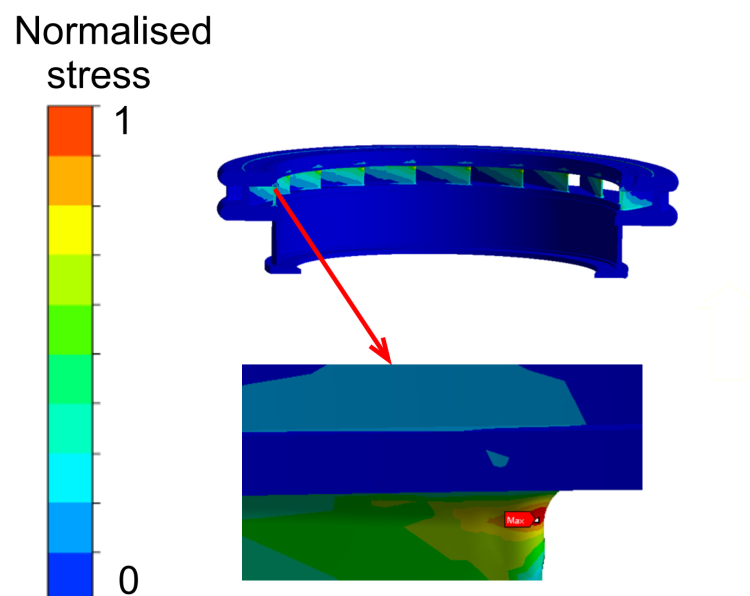


Figure 18. Stress distribution of stay ring.

The bottom ring is under less pressure due to its integral burial in the concrete. Figure 19 shows the stress distribution normalized by the maximum. The data were normalized according to the maximum stress on the bottom ring during turbine start-up. The maximum stress value of the bottom ring during the turbine start-up is 23.45 MPa,

which is lower than the material yield limit of 335 MPa. The bottom ring is considered structurally safe.

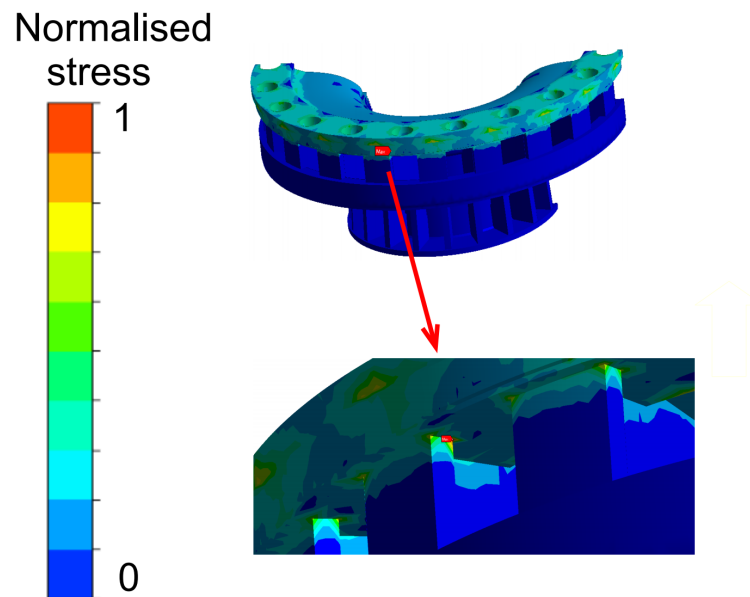


Figure 19. Stress distribution of bottom ring.

In the start-up process of a turbine, the stationary structure experiences similar stresses at different key time points. Static structures keep their stress concentration area constant, but their maximum stress value changes over time. There is a greater maximum value of stress in stay ring than in head cover and bottom ring. The stress variation in the stationary structure is normalized in comparison with the maximum stress of the stay ring, as shown in Figure 20. The data were normalized according to the maximum stress on the stay ring during the turbine start-up process.

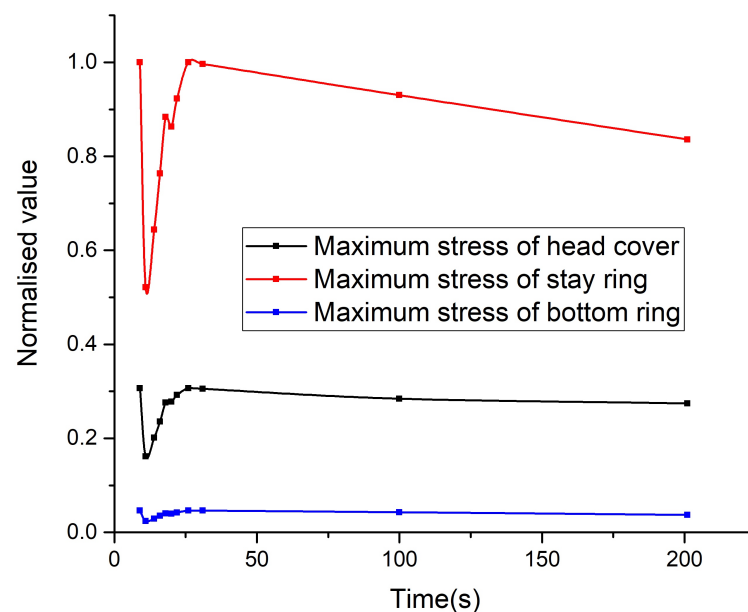


Figure 20. Comparison of the maximum stresses of three stationary structures.

Figure 21 compares the axial thrust on the head cover to the normalized maximum stress on the fixed stationary structure. The data were normalized according to the maximum value of each parameter of the turbine start-up process. Generally speaking, these

parameters follow the same trend. Axial thrust on the head cover alters the maximum stress on stay ring, bottom ring, and head cover.

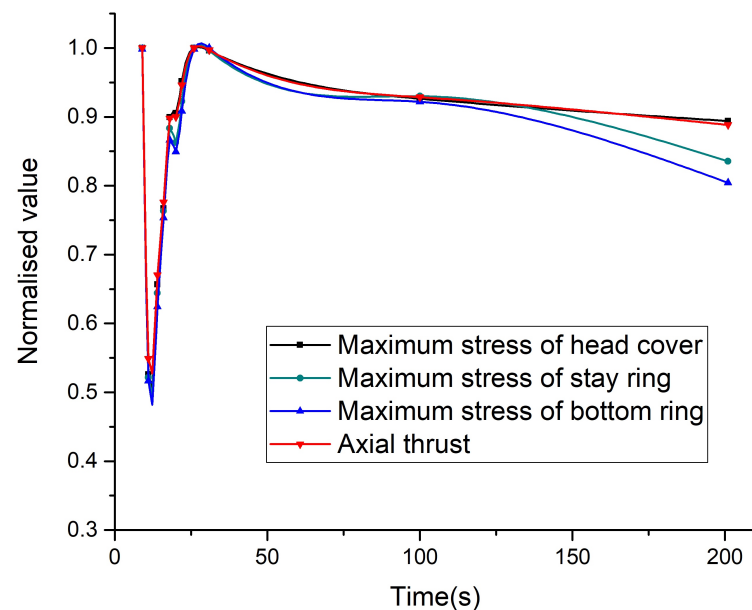


Figure 21. Results comparison during turbine start-up.

5. Conclusions

A prototype pump–turbine is analyzed in this study for its fluid dynamic and flow-induced structural behavior during turbine start-up.

When the guide vane opens, there is a rapid increase in flow rate and rotation speed. Furthermore, the pressure distribution of the runner passages gradually increases. The vaneless area between guide vanes and the runner forms a water ring, and backflow and a complex vortex structure fill the entire flow path. The flow gradually stabilizes until the increasing load stage, when the opening is gradually increased to the opening of the rated operating conditions.

With a gradual increase in flow rate and speed of rotation, the equivalent stress and deformation of the runner blade increase as well. The blade inlet side deformation is significantly greater than the blade outlet side. The maximum stress and deformation appears at the top and root of the blade's inlet side.

The trend of the deformation of the stationary structure over time is the same as the trend of the axial thrust. It is the inner head cover that experiences the greatest amount of deformation.

For the head cover, the most stress occurs at the root of the ribbed plates. For the stay ring, the maximum pressure occurs at the rounded corners on the outlet side of the stay vane. The bottom ring is under less pressure due to its integral burial in the concrete. The stay ring has a higher maximum stress value than those of the head cover and bottom ring. The maximum stress value exceeds the yield strength of the material, which may lead to structural fatigue damage during prolonged operation. The stress concentration of the stay ring can be improved by increasing the radius of the guide vanes or increasing the length or thickness of the guide vanes. The maximum stress values of head cover and bottom ring are lower than the material yield limit. So, the head cover and bottom ring are considered structurally safe. The trend of the highest level of stress of the stationary structure over time is also the same as the trend of axial thrust.

The findings of this study contribute to a better understanding of flow characteristics and structural characteristics of pump–turbine transient processes and can help to design and improve pump–turbines to ensure their safe and stable operation.

Author Contributions: Conceptualization, Z.W. and X.H.; methodology, X.Y. and X.H.; software, X.Y. and H.B.; validation, X.H., S.Z. and H.B.; investigation, X.Y. and X.H.; writing—original draft preparation, X.Y.; writing—review and editing X.Y. and X.H.; supervision, Z.W. All authors have read and agreed to the published version of the manuscript.

Funding: This research received no external funding.

Institutional Review Board Statement: Not applicable.

Informed Consent Statement: Not applicable.

Data Availability Statement: Not applicable.

Conflicts of Interest: The authors declare no conflicts of interest.

References

1. Peltier, R.; Boyko, A.; Popov, S.; Krajisnik, N. Investigating the Sayano-Shushenskaya Hydro Power Plant Disaster. *Power* **2010**, *154*, 48.
2. Casanova, F.; Mantilla, C. Fatigue failure of the bolts connecting a Francis turbine with the shaft. *Eng. Fail. Anal.* **2018**, *90*, 1–13. [[CrossRef](#)]
3. Huang, X.; Chamberland-Lauzon, J.; Oram, C.; Klopfer, A.; Ruchonnet, N. Fatigue analyses of the prototype francis runners based on site measurements and simulations. *IOP Conf. Ser. Earth Environ. Sci.* **2014**, *22*, 012014. [[CrossRef](#)]
4. Ji, X.Y.; Li, X.B.; Su, W.T.; Lai, X.; Zhao, T.X. On the hydraulic axial thrust of francis hydro-turbine. *J. Mech. Ence. Technol.* **2016**, *30*, 2029–2035. [[CrossRef](#)]
5. Egusquiza, E.; Valero, C.; Huang, X.; Jou, E.; Guardo, A.; Rodriguez, C. Failure investigation of a large pump-turbine runner. *Eng. Fail. Anal.* **2012**, *23*, 27–34. [[CrossRef](#)]
6. Luna-Ramirez, A.; Campos-Amezcuca, A.; Dorantes-Gomez, O.; Mazur-Czerwicz, Z.; Muñoz-Quezada, R. Failure Analysis of Runner Blades in a Francis Hydraulic Turbine—Case Study. *Eng. Fail. Anal.* **2016**, *59*, 314–325. [[CrossRef](#)]
7. Frunzaverde, D.; Muntean, S.; Marginean, G.; Campian, V.; Maravina, L.; Terzi, R.; Serban, V. Failure analysis of a francis turbine runner. *IOP Conf. Ser. Earth Environ. Sci.* **2010**, 012115. [[CrossRef](#)]
8. Egusquiza, M.; Egusquiza, E.; Valentin, D.; Valero, C.; Presas, A. Failure investigation of a pelton turbine runner. *Eng. Fail. Anal.* **2017**, *81*, 234–244. [[CrossRef](#)]
9. Flores-Dominguez, M.; Urquiza, G.; Rodriguez, J. A Fatigue Analysis of a Hydraulic Francis Turbine Runner. *World J. Mech.* **2012**, *2*, 28–34. [[CrossRef](#)]
10. Lyutov, A.; Kryukov, A.; Cherny, S.; Chirkov, D.; Salienco, A.; Skorospelov, V.; Turuk, P. Modelling of a Francis Turbine Runner Fatigue Failure Process Caused by Fluid-Structure Interaction. *IOP Conf. Ser. Earth Environ. Sci.* **2016**, *49*, 072012. [[CrossRef](#)]
11. Liu, X.; Luo, Y.; Wang, Z. A review on fatigue damage mechanism in hydro turbines. *Renew. Sustain. Energy Rev.* **2016**, *54*, 1–14. [[CrossRef](#)]
12. Gagnon, M.; Tahan, S.A.; Bocher, P. Impact of startup scheme on francis runner life expectancy. *IOP Conf. Ser. Earth Environ. Sci.* **2010**, *12*, 012017. [[CrossRef](#)]
13. Hao, Q.; Chai, J.; Ma, C.; Ding, J.; Li, B. Causes of Header Bolt Fracture of a Pumped Storage Power Station. *J. Yangtze River Sci. Res. Inst.* **2019**, *36*, 134–138.
14. Funan, C.; Huili, B.; Soo, H.A.; Zhongyu, M.; Zhengwei, W. Investigation on dynamic stresses of pump-turbine runner during start up in turbine mode. *Processes* **2021**, *9*, 499.
15. Zhang, Y.; Zhang, Y.; Wu, Y. A review of rotating stall in reversible pump turbine. *Proc. Inst. Mech. Eng. Part J. Mech. Eng. Sci.* **2016**, *231*, 1181–1204. [[CrossRef](#)]
16. Goyal, R.; Cervantes, M.J.; Gandhi, B.K. Characteristics of Synchronous and Asynchronous modes of fluctuations in Francis turbine draft tube during load variation. *Int. J. Fluid Mach. Syst.* **2017**, *10*, 164–175. [[CrossRef](#)]
17. Ciocan, G.D.; Iliescu, M.S.; Vu, T.C.; Nennemann, B.; Avellan, F. Experimental Study and Numerical Simulation of the FLINDT Draft Tube Rotating Vortex. *J. Fluids Eng.* **2006**, *129*, 146–158. [[CrossRef](#)]
18. Kolšek, T.; Duhovnik, J.; Bergant, A. Simulation of unsteady flow and runner rotation during shut-down of an axial water turbine. *J. Hydraul. Res.* **2006**, *44*, 129–137. [[CrossRef](#)]
19. He, L.Y.; Wang, Z.W.; Kurosawa, S.; Nakahara, Y. Resonance investigation of pump-turbine during startup process. *IOP Conf. Ser. Earth Environ. Sci.* **2014**, *22*, 32024. [[CrossRef](#)]
20. Luo, Y.; Chen, F.; Chen, L.; Wang, Z.; Yu, J.; Zhu, X.; Zhao, Z.; Ren, S.; Li, J.; Lu, X. Study on Stresses of head-cover Bolts in a pump-turbine Based on FSI. *IOP Conf. Ser. Earth Environ. Sci.* **2021**, *804*, 042062. [[CrossRef](#)]
21. Wang, Z.; Yang, J.; Wang, W.; Qu, J.; Huang, X.; Zhao, W. Research on the Flow-Induced Stress Characteristics of Head-Cover Bolts of a Pump-Turbine during Turbine Start-Up. *Energies* **2022**, *15*, 1832. [[CrossRef](#)]
22. Yang, M.; Zhao, W.; Bi, H.; Yang, H.; He, Q.; Huang, X.; Wang, Z. Flow-Induced Vibration of Non-Rotating Structures of a High-Head Pump-Turbine during Start-Up in Turbine Mode. *Energies* **2022**, *15*, 8743. [[CrossRef](#)]

23. Zhang, S.; Huang, X.; Yin, X.; Bi, H.; Wang, Z. Flow Characteristics Analysis of a High-Head Prototype Pump-Turbine During Turbine Start-Up: Effects of the Clearance. *IOP Conf. Ser. Earth Environ. Sci.* **2022**, *1079*, 012036. [[CrossRef](#)]
24. Zhou, X.; Yin, X.; Wang, W.; Huang, X.; Zhang, S.; Bi, H.; Wang, Z. Flow-induced vibration analysis of a prototype pump-turbine runner during turbine start-stop transient process. *Iop Conf. Ser. Earth Environ. Sci.* **2022**, *1079*, 012073. [[CrossRef](#)]
25. Xiaoxi, Z.; Cheng, Y.; Yang, J.D.; Xia, L.S.; Lai, X. Simulation of the load rejection transient process of a francis turbine by using a 1D-3D coupling approach. *J. Hydrodyn. Ser. B.* **2014**, *26*, 715–724. [[CrossRef](#)]
26. Chen, F.; Yang, X.; Bi, H.; Mao, Z.; Luo, Y.; Fan, H.; Wang, Z. Analysis of dynamic stresses of pump-turbine runner during load rejection process in turbine mode. *IOP Conf. Ser. Earth Environ. Sci.* **2021**, *774*, 012100. [[CrossRef](#)]
27. Mao, Z.; Tao, R.; Chen, F.; Bi, H.; Cao, J.; Luo, Y.; Fan, H.; Wang, Z. Investigation of the starting-up axial hydraulic force and structure characteristics of pump turbine in pump mode. *J. Mar. Sci. Eng.* **2021**, *9*, 158. [[CrossRef](#)]
28. Nicolle, J.; Giroux, A.M.; Morissette, J.F. Cfd configurations for hydraulic turbine startup. *IOP Conf. Ser. Earth Environ. Sci.* **2014**, *22*, 032021. [[CrossRef](#)]
29. He, L.; Zhou, L.; Ahn, S.H.; Wang, Z.; Nakahara, Y.; Kurosawa, S. Evaluation of gap influence on the dynamic response behavior of pump-turbine runner. *Eng. Comput.* **2019**, *36*, 491–508. [[CrossRef](#)]
30. He, Q.; Huang, X.; Yang, M.; Yang, H.; Bi, H.; Wang, Z. Fluid–Structure Coupling Analysis of the Stationary Structures of a Prototype Pump Turbine during Load Rejection. *Energies* **2022**, *15*, 3764. [[CrossRef](#)]

Disclaimer/Publisher’s Note: The statements, opinions and data contained in all publications are solely those of the individual author(s) and contributor(s) and not of MDPI and/or the editor(s). MDPI and/or the editor(s) disclaim responsibility for any injury to people or property resulting from any ideas, methods, instructions or products referred to in the content.